BeBeC-2020-D07

COMPARISON OF CAVITY GEOMETRIES FOR A MICROPHONE ARRAY IN AN OPEN-JET WIND-TUNNEL EXPERIMENT

Colin VanDercreek[1], Roberto Merino-Martinez[1], Mirjam Snellen[1],
Daniele Ragni[1], and Dick G. Simons[1]
[1]Aircraft Noise and Climate Effects, Faculty of Aerospace Engineering, TU Delft
Kluyverweg 1, 2629 HS Delft, The Netherlands

Abstract

This paper analyses the influence of microphone cavity geometry on beamforming measurements with a turbulent boundary layer present on the microphone array. A 16-microphone array was tested in the anechoic open-jet wind tunnel of the Delft University of Technology. The array was placed on a flat plate mounted flush with the exit nozzle of the wind tunnel. Microphones were installed in three different cavity geometries along with a flush mounted microphone array which was used as a baseline for comparison. The geometries include a chamfered-cylindrical hard-plastic cavity, a chamfered-cylindrical cavity made of melamine foam, and a chamfered-cylindrical cavity with star-shaped protrusions, also made of melamine. The recessed cavities were covered with a 0.026 mm gauge steel-wire cloth. A speaker emitting white noise outside of the flow was employed as a sound source. Different flow velocities at the same sound power level for the speaker (and hence different signal-to-noise ratios) were studied. The results obtained with the three cavity geometries are compared with the flush-mounted case in terms of the quality of the acoustic source maps (location and strength of the sound source). The signal-to-noise ratio of the beamforming measurements increased by as much as 30 dB by placing microphones within a conical cavity with melamine foam walls when compared to the flush mounted case.

1 INTRODUCTION

Aeroacoustic experiments in wind tunnels are often performed in open-jet facilities because they allow for placing the microphones outside of the flow [1]. However, the aerodynamic conditions in open-jet wind tunnels [2] are less well-controlled than in closed-section wind tunnels. Acoustic measurements in closed-section wind tunnels, on the other hand, are affected

by several sources of noise inherent to wind tunnels [3], these include the turbulent boundary layer (TBL) along the tunnel's walls, the tunnel machinery and reflections that propagate within the tunnel. To reduce the amount of flow noise measured, microphones should be placed in a non-intrusive manner to avoid additional noise generation because of the interaction with the flow [4]. The present manuscript focuses on minimizing the influence of the TBL along the microphone array on the acoustic beamforming measurements.

The signal-to-noise ratio (SNR) of the microphone arrays can be increased by attenuating the level of TBL noise, which can be achieved in two main ways: 1) by employing acoustic beamforming and removing the main diagonal of the cross-spectral matrix (CSM), which averages out the incoherent noise, such as TBL noise [5], and 2) by placing the microphones within cavities [6–8]. The latter is commonly done by recessing microphones behind an acoustically transparent material (such as a stainless steel cloth or a Kevlar sheet), which reduces the convection of the hydrodynamic pressure fluctuations of the boundary layer into the cavity but allows for the propagation of acoustic waves. The geometry of the cavity itself has a significant effect on the amount of attenuation. Previous research [6, 7, 9, 10] showed the benefit of these cavities in acoustic array measurements, but little work [7, 9, 11] has been done in quantifying the differences in TBL noise attenuation and SNR increase due to the cavity for a given array. This paper aims to quantify the impact different cavities have on beamforming measurements by comparing three different cavity geometries with a flush mounted array, for the same microphone array distribution.

The shape and cavity wall material have significant influence on cavity performance with respect to TBL attenuation [6, 8]. The following geometric parameters influence the cavity performance: cavity depth, cavity aperture area, aperture area reduction with respect to depth, wall material, and the presence of an acoustically transparent material (in this case a stainless steel wire cloth) over the top of the cavity.

The primary physical mechanism for reducing the TBL noise is the fact that, given that the diameters of the cavities are on the order of 10 mm and the frequency range of interest between 250 Hz and 10 kHz, the majority of acoustic modes, excited at the aperture by the hydrodynamic waves, within the cavity are cut-off and, therefore, non-propagating [12]. The boundary layer energy is spread out across many acoustic modes, with a dependency on frequency. This energy shifts towards higher order modes with increasing frequency. For the non-propagating or cut-off modes, the TBL energy attenuates exponentially. Whether a mode is propagating or not is determined by the aperture area and the wavenumber. Therefore with increasing cavity depth, the TBL energy is attenuated before it is measured by the microphone. This effect is minimal at low frequencies but is more pronounced at higher frequencies. Reducing the area with increasing depth is another effective way to attenuate the TBL noise due to the fact that the change in area results in a transmission loss for the propagating wave. Cavity walls made of absorbing materials, such as melamine, reduce the intensity of reflections and standing wave amplitudes within the cavity, resulting in a further reduction in the TBL noise at the microphone. Finally, covering the cavity with an acoustically transparent material, such as a fine stainless steel wire cloth or a Kevlar sheet [7, 13], reduces the effect of the hydrodynamic fluctuations of the boundary layer, resulting in as much as a 10 dB additional reduction in TBL noise at the microphones. The cavities in this study have both hard and soft walls, a stainless steel cloth covering, and different depths and aperture areas.

Conventional frequency domain beamforming (CFDBF) [14] was employed to evaluate the

interaction between the TBL over the array and different cavities while measuring a single speaker emitting a white noise signal. Beamforming is used to locate and quantify the sound pressure level (SPL) of the sound sources. Since TBL noise is assumed to be incoherent from microphone to microphone [15], beamforming improves the SNR of the measurements by reducing this noise source. Additionally, diagonal removal (DR) can be used to further reduce this noise. It should be noted that, whereas the use of some advanced acoustic imaging algorithms [16–18] can also reduce the effect of TBL and background noise, most of them rely on the results of conventional beamforming. Thus, this paper only considers conventional beamforming results, since improving these is also expected to, consequently, improve the results of advanced methods.

The measurements were performed at the anechoic open-jet wind tunnel of Delft University of Technology (A-Tunnel) [19] where a microphone array used to measure a speaker located just outside of the airflow. Measurements were made for flow velocities U_∞ of 20.2 and 34.2 $\mathrm{m\,s^{-1}}$ without the speaker and with the speaker emitting a white noise signal.

The objectives of this experiment are to (1) quantify the SNR improvement due to different cavities coupled with post-processing on beamforming, and (2) generate a data set of different microphone cavities to support future model development to improve the signal to noise ratio (SNR) of acoustic measurements.

2 EXPERIMENTAL SET-UP

2.1 Wind Tunnel Set-up

The test section of the A-Tunnel is located in an anechoic plenum covered with acoustic absorbing foam wedges, which provides free-field sound propagation properties for frequencies higher than 200 Hz [19], i.e., it avoids unwanted reflections from walls, floor and ceiling. An open-jet wind tunnel was selected so that the primary noise source would be the TBL over the array and to be able to place a known reference sound source outside of the flow, avoiding the interaction of the flow with the sound source. This setup mimics the microphone situation inside of a closed-section wind tunnel. The rectangular nozzle employed has an exit area of 0.7 m $\times$ 0.4 m, see Fig. 1a, and provides a maximum flow velocity U_∞ of 34.2 $\mathrm{m\,s^{-1}}$. For this experiment flow velocities of 20.2 and 34.2 $\mathrm{m\,s^{-1}}$ were considered.

2.2 Microphone Array

The acoustic array employed consists of 16 microphones with two additional flush mounted reference microphones. These 16 microphones were placed in a sunflower pattern [20] with an array diameter of 350 mm as seen in Fig. 1b. The layout was optimized [21] to minimize sidelobes and maximize the dynamic range between the frequencies of 2 kHz and 4 kHz. This design was predicted to have a maximum dynamic range of 9.6 dB.

G.R.A.S. 40PH analog free-field microphones [22] were used in the array which feature an integrated constant current power (CCP) amplifiers, and a 135 dB dynamic range. Each microphone has a diameter of 7 mm and a length of 59.1 mm. All the microphones were calibrated individually using a *G.R.A.S. 42AA* pistonphone [23]. The transducers have a flat frequency response within $\pm$1 dB from 50 Hz to 5 kHz and within $\pm$2 dB from 5 kHz to 20 kHz. The data acquisition system consisted of 4 *National Instruments* (NI) *PXIe-4499* sound and vibration

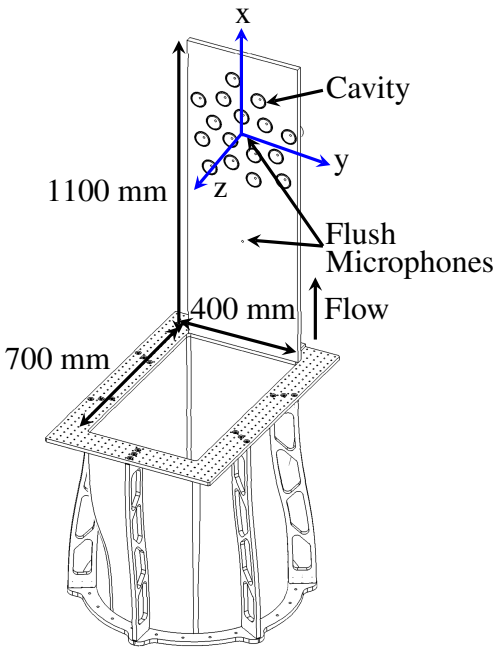

(a) Mounted Array

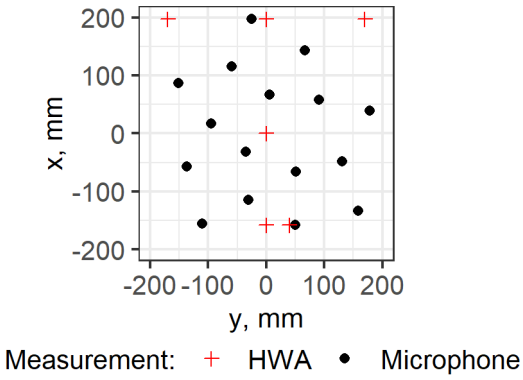

(b) Array layout

Figure 1: Experimental set-up at the A-Tunnel. a.) Array mounted on nozzle. b.) Array microphone distribution with hot-wire anemometry measurement locations as seen from in front.

modules with 24 bits resolution. The boards are controlled by a NI *RMC-8354* computer via a NI *PXIe-8370* board.

The array was installed in a 1.1 m $\times$ 0.4 m poly-carbonate plate, see Fig. 1a. Two different plates were manufactured: one with 7 mm diameter holes for the flush mounted microphones (Array 1) and another one that is covered with a #500 stainless steel cloth with an aperture of 0.026 mm and thread size of 0.025 mm. The second plate features 16 threaded holes of 50 mm diameter at the microphone positions, which allowed for different cavity inserts to be installed. This second plate was used for arrays 2, 3 and 4. The center of the microphone distribution ($x = y = 0$) is located 800 mm downstream of the nozzle outlet in order to allow for the boundary layer to become fully turbulent. Both plates feature two additional flush mounted microphones mounted along the array center line, $y = 0$ according to the coordinate system defined in Fig. 1a. These microphones were used as a reference measurement to compare against the cavity measurements.

2.3 Cavity Design

Three different cavity geometries were compared against the baseline flush mounted microphone array, array 1, which features 16 circular holes machined in the poly-carbonate plate with the exact diameter of the *G.R.A.S. 40PH* microphone (7 mm).

An example cavity holder is illustrated in Fig. 2. The cavity for array 2 is made of a poly-

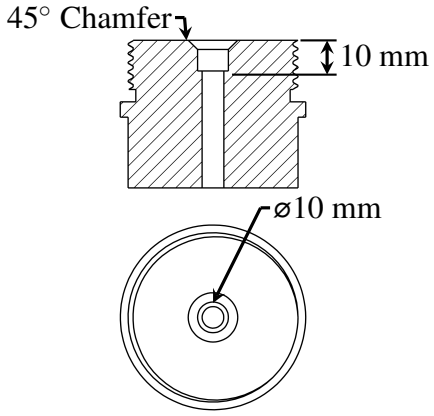

Figure 2: Example shape and dimensions of the hard walled cavity used in array 2 for this experiment. All three cavities were mounted in similar holders.

carbonate material and, therefore, features hard walls. It also features a 45° chamfer at the top and has a diameter of 10 mm and a depth of 10 mm. This geometry was chosen based on it being the most effective shape for attenuating TBL noise in a previous experiment [8].

The cavity for array 3 features soft walls made of melamine foam. It has a conical shape and features 10 evenly distributed ridges. The ridges were included to study whether they would better attenuate azimuthal modes [24] compared to a perfectly conical cavity. Array 4 features cavities made of melamine foam with the same conical geometry as cavity 3 but without the ridges. The cavities of arrays 3 and 4 were installed in a threaded poly-carbonate insert with the same outer mold line as those from array 2. The cavities of arrays 2, 3 and 4 were covered with the aforementioned stainless steel cloth.

2.4 Hot-Wire Anemometry (HWA)

The boundary layer was not tripped. To verify that the boundary layer was turbulent and attached, especially near the upper edges of the plate, Hot-Wire Anemometry (HWA) measurements were made at 6 locations and at flow speeds of 10, 20.2, and 34.2 $\mathrm{m\,s^{-1}}$. These measurements were performed at three points along the top of the plate, two points along the center-line, and at one point just over a cavity, see Fig. 1b. The coordinates of these points are contained in Table 1 using the coordinate system defined in Fig. 1a. A calibrated *Dantec* 1-channel hot-wire probe was used. The sampling frequency was 50 kHz with a 10 kHz low-pass filter with a 3% measurement uncertainty. These measurements were performed for both the baseline flush mounted array which was made of smooth poly-carbonate and for the other arrays which were covered by a stainless steel cloth to determine whether this cloth affected the boundary layer.

2.5 Acoustic Measurements

A single Visaton K 50 SQ speaker [25] was mounted at a distance 800 mm normal to the array, 650 mm downstream from the nozzle outlet (at $x = -150$ mm), and aligned with the axis of the jet. The speaker has a baffle diameter of 45 mm and was located just outside of the flow to avoid additional noise sources due to the impingement of the shear layer. The speaker was used

to emit white noise with an overall sound pressure level (OSPL), measured at the array location, of 64 dB. Figure 3 depicts the one-third-octave bands spectrum of the speaker signal measured by Array 1, as well as the background noise of the facility.

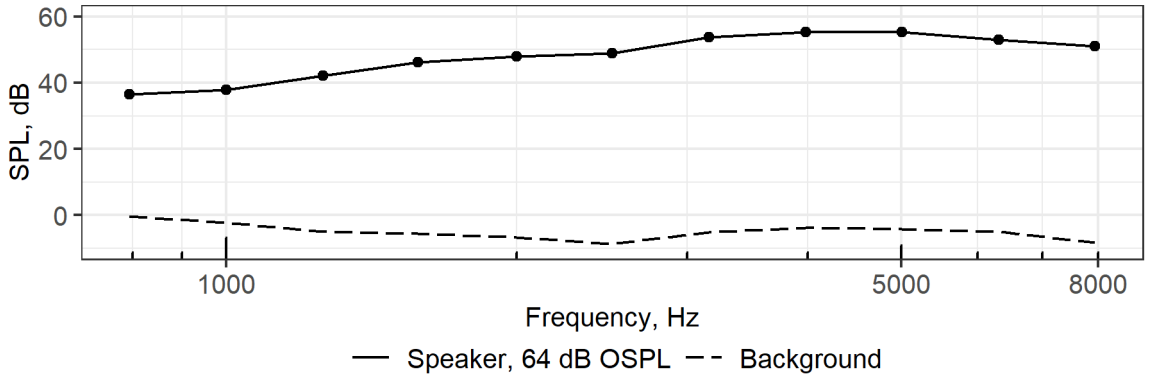

Figure 3: Speaker output spectrum in one-third-octave bands as measured at the reference array, Array 1, with background noise levels as reference.

The sampling frequency of the recordings was 51.2 kHz. The signal was sampled for a duration of 45 s. CFDBF was applied to the acoustic data, with and without DR. The CSM was calculated using 5120 samples with a 50 % overlap using the Hanning window. The scan grid is located 0.8 m from the array in the z direction, i.e. at the speaker plane, and centered to the origin of the coordinate reference system shown in Fig. 1a. The scan grid is 0.6 m $\times$ 0.6 m with a spacing between scan points of $\Delta x = \Delta y = 0.01$ m. The quantitative frequency spectrum was obtained using the Sound Power Integration (SPI) technique [15, 18, 26, 27]. The results obtained were used to evaluate the resulting beam width, side lobe level, attenuation of the TBL noise, and resulting SNR for the measurements of the speaker.

3 EXPERIMENTAL RESULTS

3.1 Boundary Layer Measurements

A summary of the boundary layer statistics for the plate of arrays 2-4 (poly-carbonate covered with stainless steel cloth) at a flow velocity of $U_\infty = 20.2\,\mathrm{m\,s^{-1}}$ is shown in Table 1. These results show that the boundary layer is turbulent over the microphone array, defined as having a shape factor, H, around 1.3 to 1.4. The boundary layer measurements for the $U_\infty = 34.2\,\mathrm{m\,s^{-1}}$ (not shown here) were consistent with the $U_\infty = 20.2\,\mathrm{m\,s^{-1}}$ case. These results show that the boundary layer is reasonably consistent at the extreme upper corners of the array (points 4 and 6). A comparison between the smooth poly-carbonate plate of array 1 and the plate with the stainless steel cloth used for arrays 2, 3 and 4 showed no significant differences with respect to the boundary layer characteristics.

3.2 Acoustic source maps

The beam width and sidelobe level (dynamic range) were calculated for each array and for the following velocities: no flow, $20.2\,\mathrm{m\,s^{-1}}$, and $34.2\,\mathrm{m\,s^{-1}}$. Figure 4 shows the acoustic source

Table 1: Hot-Wire Anemometry measurements locations with boundary layer statistics for the $U_\infty = 20.2\,\mathrm{m\,s^{-1}}$ case.

	Point 1	Point 2	Point 3	Point 4	Point 5	Point 6
x - position, mm	-158	-158	0	197	197	197
y - position, mm	40	0	0	0	-170	170
δ_{99}, mm	29.4	27.7	33.0	31.8	44.5	39.2
δ^*, mm	4.21	3.74	4.94	4.49	3.59	4.42
Θ, mm	3.23	2.95	3.75	3.45	2.96	3.58
H	1.3	1.27	1.32	1.30	1.21	1.23

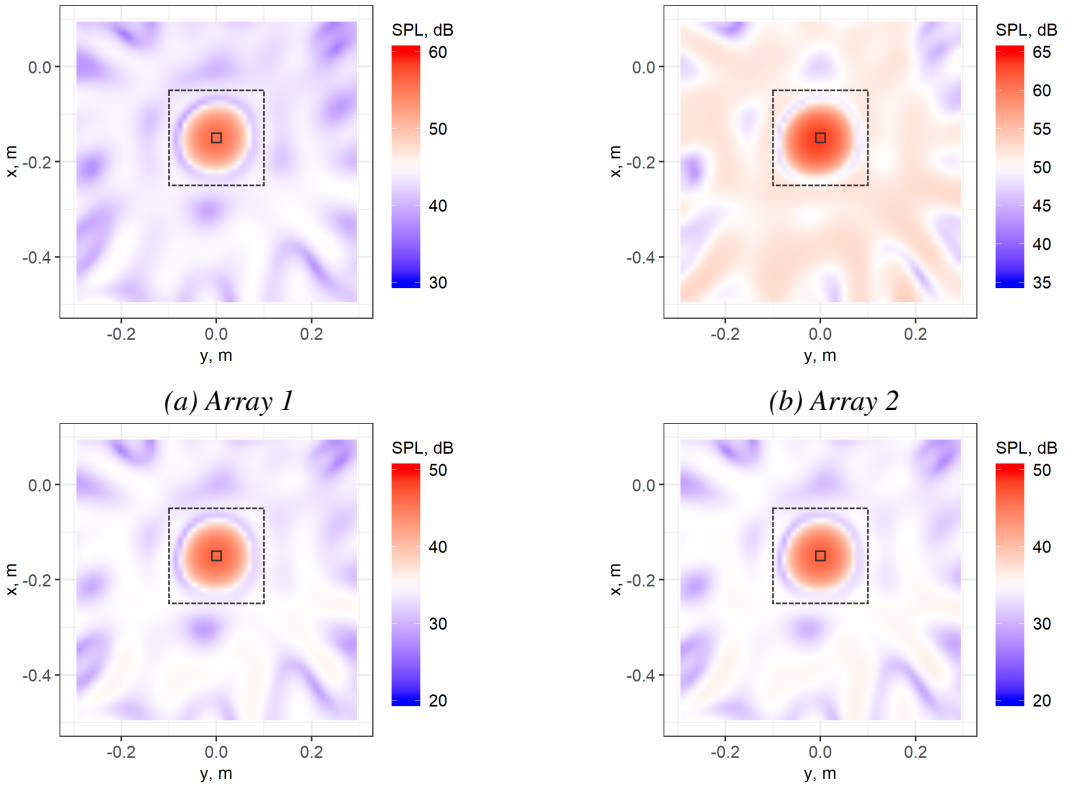

(a) Array 1 *(b) Array 2*

(c) Array 3 *(d) Array 4*

Figure 4: CFDBF source maps for the case with no flow and at a one-third-octave band centered at 8000 Hz. Solid black square represents the speaker location. The larger square with dashed lines is the region of integration.

maps of the speaker without flow for the one-third-octave band centered at 8000 Hz. In these subfigures, the solid black rectangle represents the position of the speaker (located at (x, y, z) = (0, -0.15, 0.8) m) and the dashed box denotes the limits of the region of integration (ROI) considered for SPI, which is 0.2 m by 0.2 m centered at the speaker position. Array 2 shows an

8 dB amplification with respect to array 1, most likely due to standing waves within the hard walled cavity. This is shown in Fig. 5, where the measured acoustic signal for each array is compared with a free-field measurement of the speaker, i.e. a single microphone not installed on a plate. Array 1 shows an approximate 6 dB increase across the frequency bands below 8 kHz with respect to the free-field measurement. This is due to the doubling effect at the microphone due to the sound wave reflecting off of the plate. The acoustic source levels as measured by arrays 3 and 4 are attenuated by 6 dB compared with array 1, due to the presence of the stainless steel cloth covering and because the acoustic plane wave no longer perfectly reflects off the array. These differences are more noticeable for frequencies higher than 2 kHz.

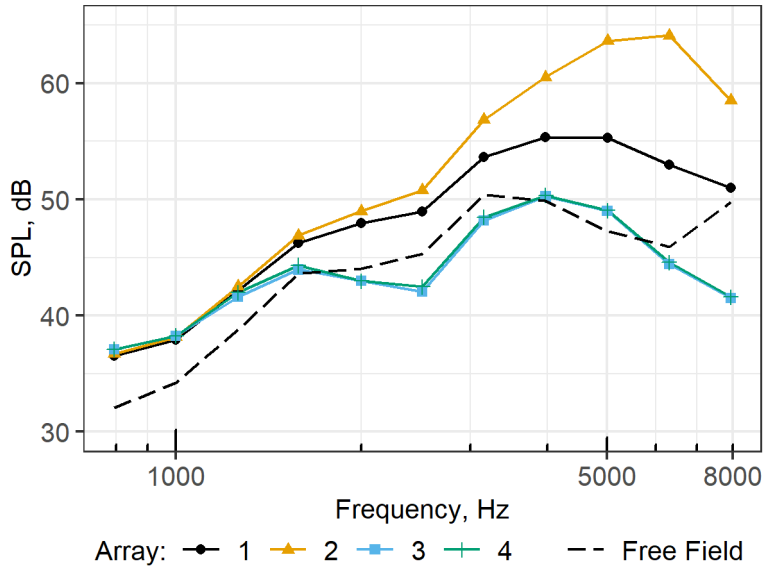

Figure 5: Effect of cavity geometry on integrated acoustic measurements, no flow, compared with free field microphone measurement.

Figure 6 compares the beam width of the main lobe 3 dB below its peak for each array [28]. This was compared with the Rayleigh spatial resolution limit [29], defined by $\Delta R = \frac{1.22hc}{fD}$, where h is the distance from the array to the source (in this case 0.8 m), c is the speed of sound, f is the sound frequency, and D is the array diameter (in this case 0.35 m). For all arrays and for the no-flow case the beam width and the Rayleigh resolution limit are in good agreement with each other for frequencies above 1 kHz. For the cases with flow, the results do not converge until the TBL noise level is below the acoustic source level, which depends on the cavity geometry. This is the reason why Fig. 6 shows discontinuities for all arrays at frequencies below 2 kHz for the 34.2 $\mathrm{m\,s^{-1}}$ case. This figure shows that for the 34.2 $\mathrm{m\,s^{-1}}$ case, array 1 does not converge until 5 kHz, array 2 does not converge until 2.5 kHz and that arrays 3 and 4 with their similar geometry converge at around 2 kHz.

Figure 7 shows the dynamic range of each array. The dynamic range was calculated as the difference between the SPL at the speaker position and the maximum sidelobe strength (outside of the main lobe): $\Delta SPL = SPL_{max}(speaker) - SPL_{max}(outside)$. The dynamic range for all four arrays is in close agreement for the no flow case. As the velocity increases, the performance diverges. Array 1, the flush mounted array, can only detect the source above 3 kHz

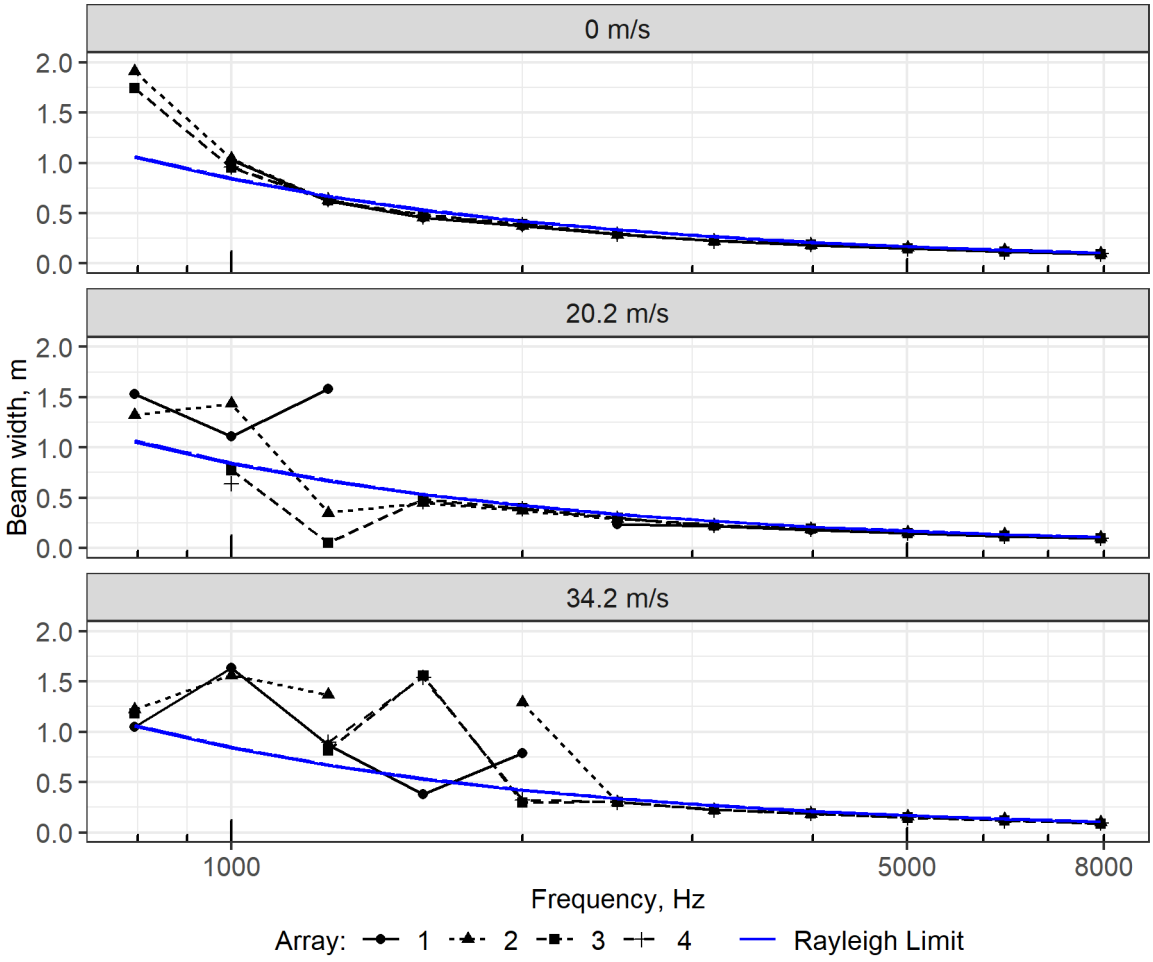

Figure 6: Beam width vs. frequency for each array, in one-third-octave bands with DR.

for the 20.2 $\mathrm{m\,s^{-1}}$ case and cannot detect it at all for the 34.2 $\mathrm{m\,s^{-1}}$ case. Array 2 performs similarly to arrays 3 and 4, but arrays 3 and 4 have a higher dynamic range at a lower frequency due to the increased TBL noise attenuation for the 34.2 $\mathrm{m\,s^{-1}}$ case. Array 2 detects the source starting at 2.5 kHz, while arrays 3 and 4 detect the source starting at 2 kHz for the 34.2 $\mathrm{m\,s^{-1}}$ case.

It should be noted that the dynamic range and beam width are primarily a function of the microphone distribution of the array. In practice, larger arrays with more microphones would provide better results in both aspects [30]. However, the intention of this work is to compare the relative effect of the cavities in the results for a given microphone distribution and not to design an optimal microphone arrangement.

Figure 8 shows the beamforming source maps (with DR) for the case with flow present over the plate. The wind tunnel flow speed was 34.2 $\mathrm{m\,s^{-1}}$. Array 1 (Fig. 8a) is unable to identify the speaker due to the TBL waves impinging on the flush mounted microphones, overwhelming the acoustic signal of the source. Arrays 2-4 are capable of identifying the speaker location as their cavity geometries attenuate the TBL noise sufficiently. The source map of array 2 shows a higher *noise floor* than the maps of arrays 3 and 4, and peak levels about 15 dB higher.

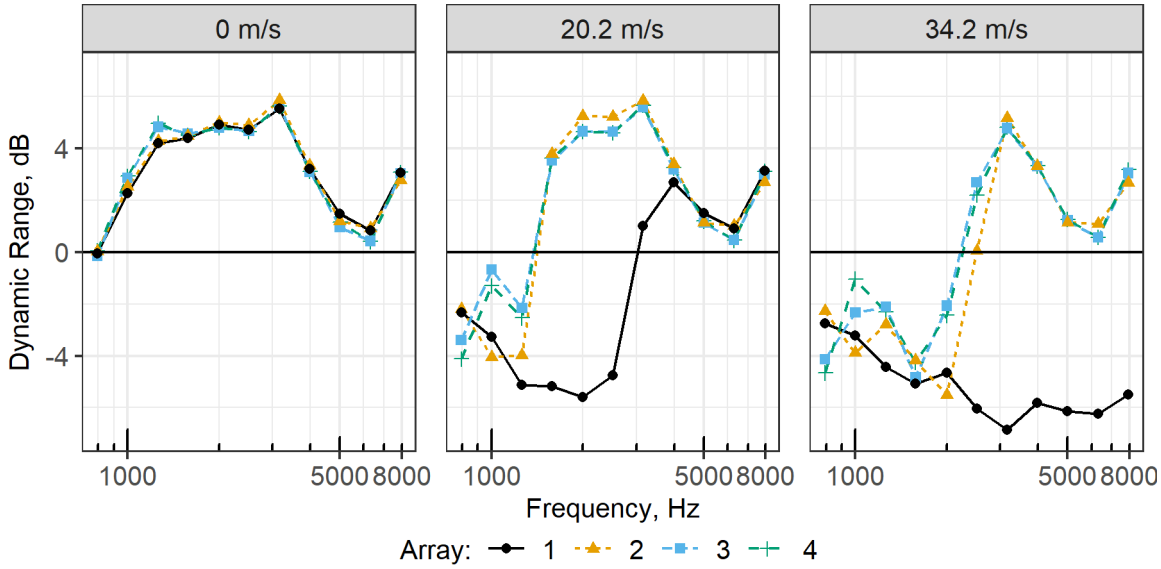

Figure 7: Dynamic range of each array, third octave bands for the low speaker output case and no flow. Conventional beamforming performed with DR.

3.3 Turbulent Boundary Layer Noise Attenuation

The pressure fluctuations of the TBL are assumed to be random and incoherent over the distances typically seen between microphones in acoustic arrays [15]. The levels of incoherent fluctuations are suppressed by beamforming which is beneficial for aeroacoustic measurements in wind tunnels, because the wind-tunnel's TBL noise is reduced with respect to the acoustic waves from the test article. This improvement can be observed in Fig. 9, where the Power Spectral Density (PSD) of the TBL as measured by the array using CFDBF (at the same scan grid location as the measurements containing the speaker), is compared with a flush mounted reference microphone and a single microphone, (Mic. 1, located at $(x,y) = (-32,-35)$ mm), near the reference microphone, for the four arrays. These measurements were made without the acoustic source. The spectra in Fig. 9 are calculated without diagonal removal and, thus, show the reduction in noise due to beamforming alone. The beamforming results of array 1 provide an 11 dB reduction in TBL noise at 2500 Hz compared with the flush mounted microphone. This is in agreement to the predicted reduction of 8 dB by Horne *et al.* [31]. Placing the microphones in cavities further attenuates this noise. Array 2 reduces the TBL noise of the single microphone by 19 dB at 2500 Hz compared to the flush mounted microphone. Arrays 3 and 4 further improve upon this with a reduction of 40 dB at 2500 Hz, compared to the flush mounted microphone. Using the entire 16 microphone array and CFDBF results in an additional improvement of 9 dB compared to a single microphone in a cavity.

Removing the diagonal of the CSM in the CFDBF processing further reduces the TBL noise spectra. Figure 10 shows the improvement over Fig. 9 due to the diagonal removal. This further reduces the effect of incoherent noise sources, such as TBL noise, which further reduces the TBL noise by an additional 25 dB at 2500 Hz for array 1, by 21 dB for array 2, and by 19 dB for arrays 3 and 4, with respect to the case without DR.

Reducing the TBL noise improves beamforming measurements by lowering the noise floor

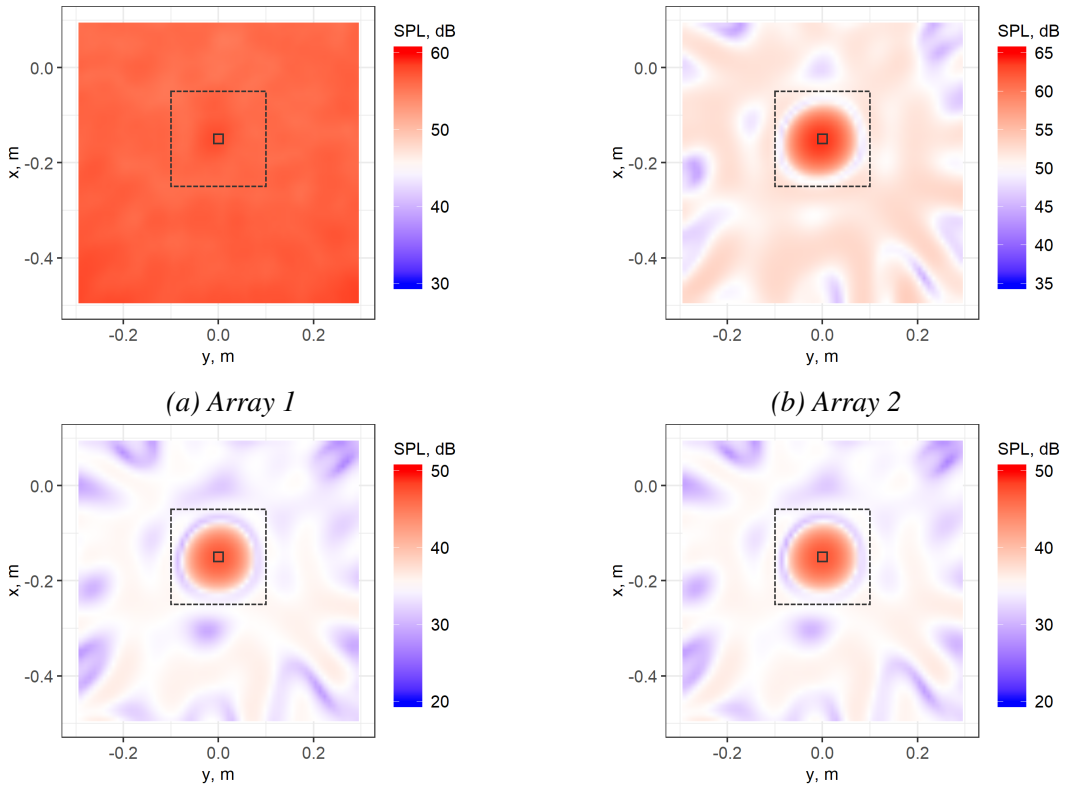

(a) Array 1 *(b) Array 2*

(c) Array 3 *(d) Array 4*

Figure 8: CFDBF source maps (with DR) for the case with $U_\infty = 32.2\,\mathrm{m\,s^{-1}}$ at a 8000 Hz one-third-octave band. Solid black square represents the speaker location. The larger square with dashed lines is the region of integration.

and thus enables the measurement of acoustic sources with lower sound power levels. Figure 11 shows the sound spectra obtained with SPI of the ROI containing the speaker for each array at the different flow speeds. DR was not applied in this case. The no-flow case contains the acoustic signal that, ideally, an array with an optimal cavity design could measure even for the cases with flow. This is illustrated by the dashed line. The lower the frequency that the measurement with flow converges on the no flow case, the better the cavity performs. The noise floor generated by the TBL is sufficiently high that array 1 cannot distinguish the signal of the speaker from the TBL noise for either the cases with a flow speed of $20.2\,\mathrm{m\,s^{-1}}$ or $34.2\,\mathrm{m\,s^{-1}}$. Array 2 improves upon these results and detects the source beginning at 2 kHz and 3.5 kHz for the $20.2\,\mathrm{m\,s^{-1}}$ and $34.2\,\mathrm{m\,s^{-1}}$ cases, respectively. The aforementioned amplification of the results by 8 dB of array 2 due to the assumed presence of standing waves is again observed in this figure. Arrays 3 and 4 lower the noise floor even further resulting in the detection of the speaker beginning at 1.4 kHz and 2.6 kHz for the $20.2\,\mathrm{m\,s^{-1}}$ and $34.2\,\mathrm{m\,s^{-1}}$ cases, respectively.

Figure 12 quantifies the improvement to acoustic measurements when the diagonal of the CSM is removed. Array 1 can now measure the source for the $20.2\,\mathrm{m\,s^{-1}}$ case starting at 2000 Hz but the noise floor is still too high to measure the source at all for the $34.2\,\mathrm{m\,s^{-1}}$ case. Arrays 2-4 further improve the source measurement by being able to measure the source

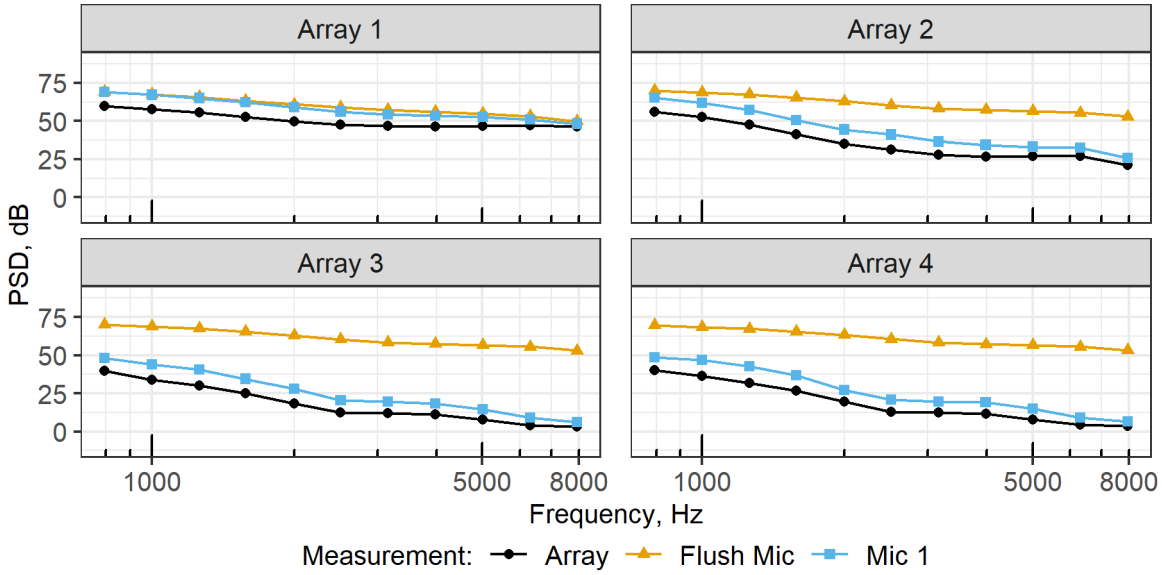

Figure 9: PSD of the TBL noise over the array without DR, U_∞ = 34.2 m/second without the acoustic source.

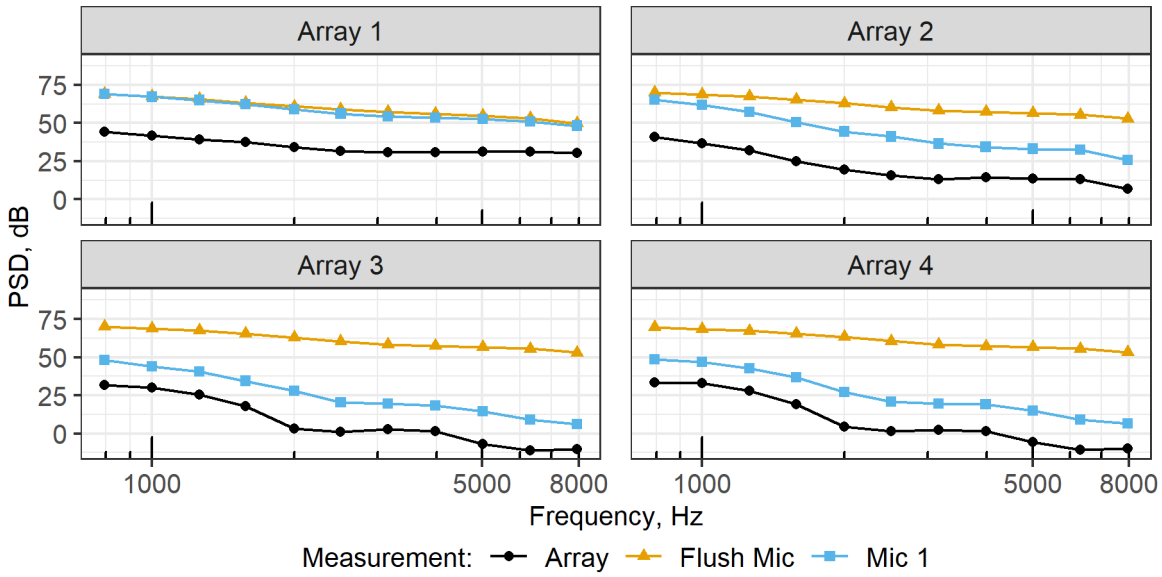

Figure 10: PSD of the TBL noise over the array with DR, U_∞ = 34.2 m/sec without the acoustic source.

at lower SPL levels which occurs at lower frequencies. These data show that beamforming measurements are further improved by using microphones within cavities.

Reducing the measured TBL noise by using cavities improves acoustic measurements. However, these cavities also affect the measurement of the acoustic signal. Figures 11 and 12 show that for the no-flow case, the integrated SPL of the source is affected by the cavities. The hard wall cavities in Array 2 amplify the acoustic signal approximately 8 dB at higher frequencies

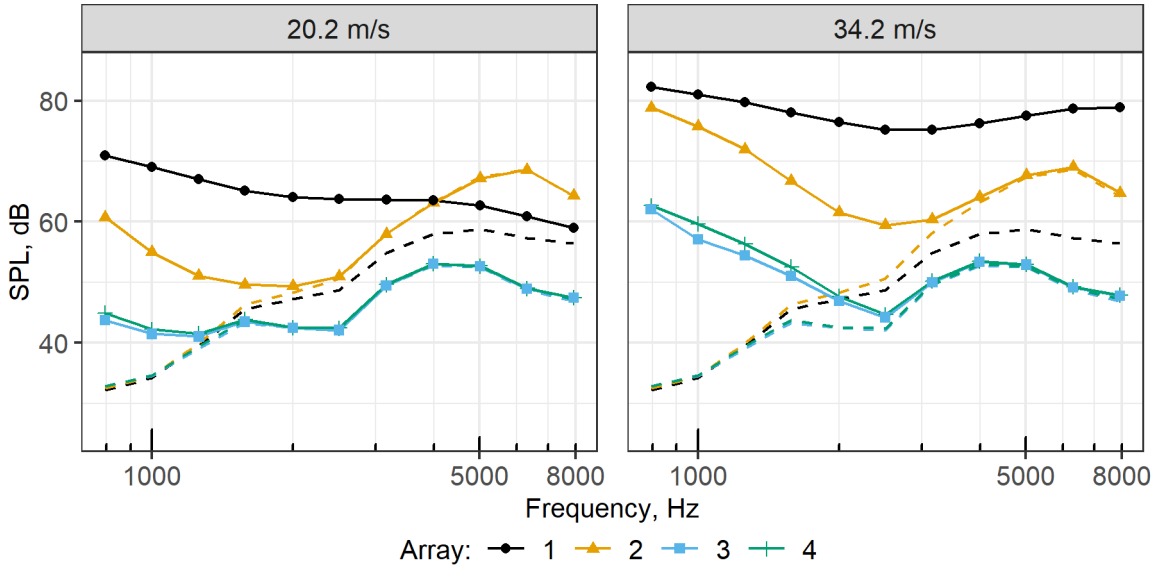

Figure 11: Integrated sound spectra for the ROI containing the speaker at different flow velocities without DR. Spectra are shown in one-third-octave bands. The dashed lines are the measurements made without flow for each array which is the ideal case.

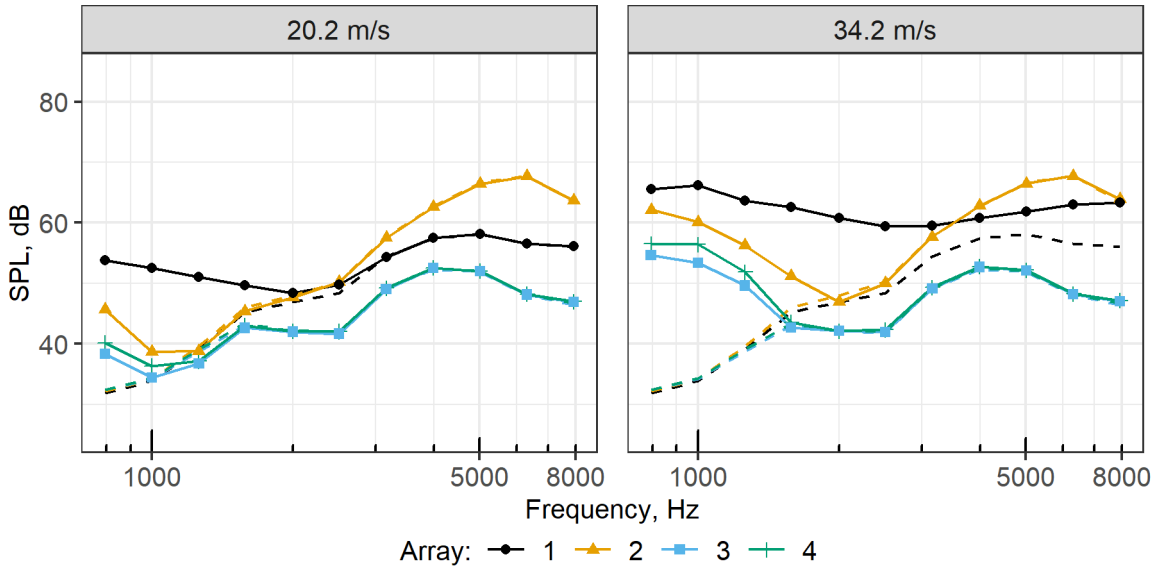

Figure 12: Integrated sound spectra for the ROI containing the speaker at different flow velocities with DR. Spectra are shown in one-third-octave bands. The dashed lines are the measurements made without flow for each array which is the ideal case.

compared to array 1. In contrast, the sound absorbing walls of arrays 3 and 4 reduce the signal by about 6 dB. Therefore, the impact of the cavities on the SNR of the array needs to be examined.

3.4 Signal-to-Noise Ratio (SNR) Improvement

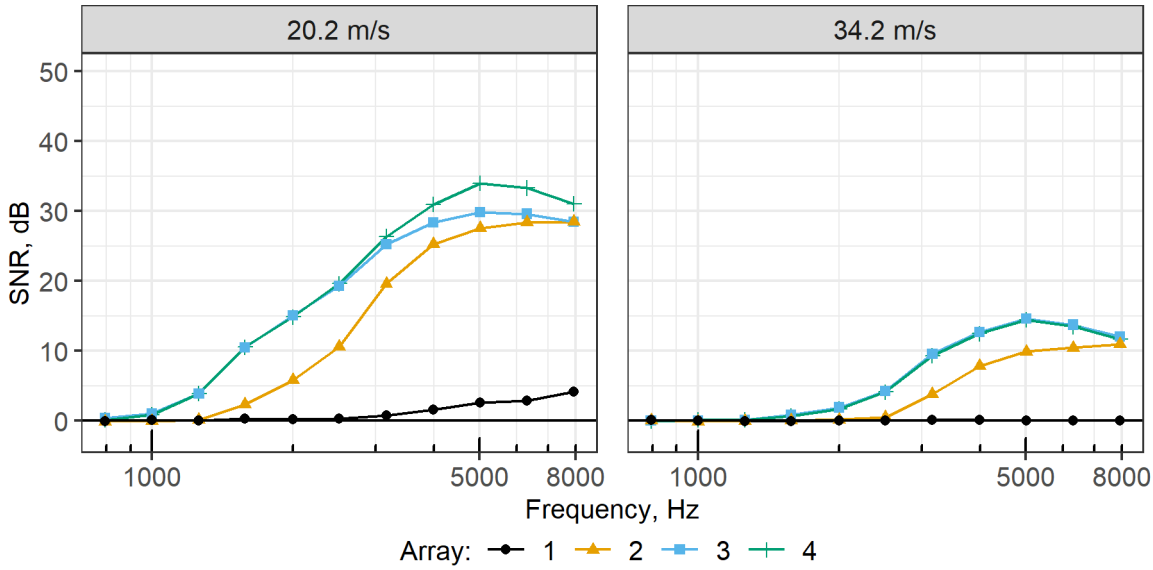

Figure 13: SNR at different flow velocities without DR. Data are plotted in one-third-octave bands.

Figure 13 shows the SNR with respect to frequency in one-third-octave bands for the four arrays and the two flow velocities. The SNR was calculated by the following expression $SNR(f) = SPI_{source}(f) - SPI_{TBL}(f)$. As discussed previously, array 1 does not attenuate the TBL noise, therefore, it has an extremely low SNR reaching a maximum value of only 5 dB at 8000 Hz. Arrays 2, 3, and 4 perform in a similar manner with a maximum SNR of 30 to 35 dB for the 20.2 $\mathrm{m\,s^{-1}}$ case. Arrays 3 and 4 perform better than Array 2 at frequencies below 3150 Hz due to their better attenuation of TBL noise. The SNR of array 2 is inflated by the fact that the measured acoustic source level is amplified by standing waves. This amplification appears to only affect the acoustic waves from the source and not the TBL waves since Fig. 9 shows no amplification of the TBL noise spectra.

Applying DR further improves the SNR of the beamforming measurements, see Fig. 14. DR increases the SNR of array 1 to approximately 15 dB for the 20.2 $\mathrm{m\,s^{-1}}$ case. However, the SNR for the 34.2 $\mathrm{m\,s^{-1}}$ is still close to zero. For the 20.2 $\mathrm{m\,s^{-1}}$ case arrays 2 and 3 still have an SNR of 30 dB but the range where this SNR is obtained starts at a much lower frequency. The 34.2 $\mathrm{m\,s^{-1}}$ case shows a significant improvement in SNR compared to the case without DR. Interestingly, Array 4 shows a 20 dB improvement in SNR compared to array 3 for the 20.2 $\mathrm{m\,s^{-1}}$ case despite the cavity geometry being relatively similar. This is due to the diagonal removal reducing the TBL noise to -20 dB, 10 dB less than array 3, for the 20.2 $\mathrm{m\,s^{-1}}$ case. The explanation for this phenomenon requires additional study.

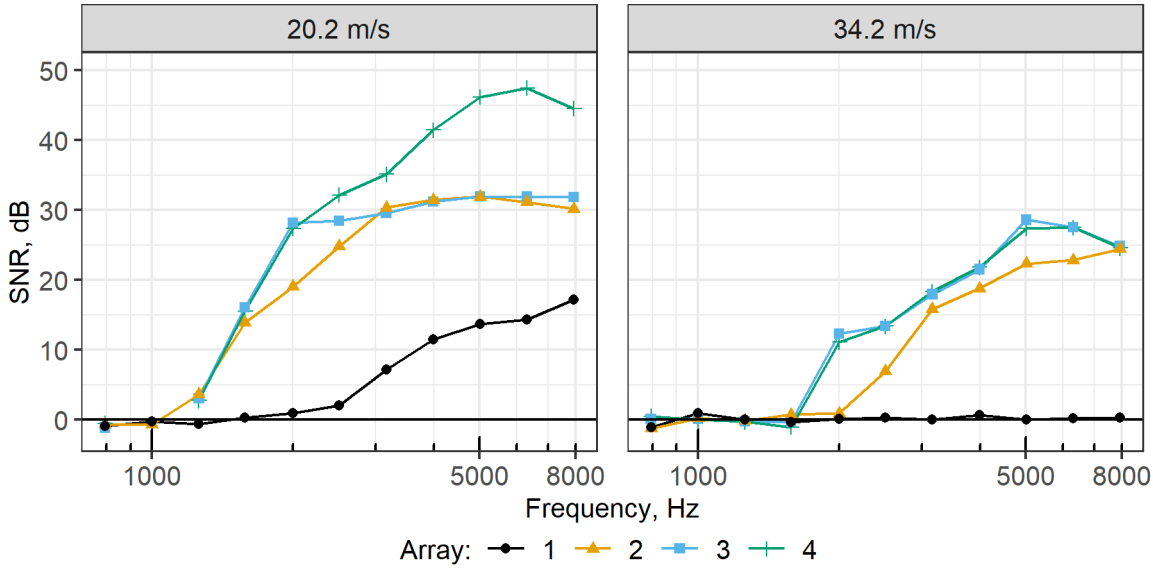

Figure 14: SNR at different flow velocities with DR. Data are plotted in one-third-octave bands.

4 CONCLUSION AND FUTURE WORK

This paper compares the effect of different microphone cavity geometries on acoustic beamforming results when a turbulent boundary layer is present over a microphone array. Four cavity geometries were compared using an array featuring 16 microphones arranged in the same sunflower distribution. These four arrays measured the same acoustic source at different velocities.

The results quantify the effect of different cavity geometries on the beamforming results. Inline with previous experiments, cavities attenuated the TBL with respect to a baseline flush mounted microphone array. It was shown that the effect of cavities in combination with diagonal removal attenuate the TBL more than by simply using diagonal removal with a flush mounted microphone array. Specifically, diagonal removal reduced the TBL noise by an additional 9 dB on top of the effect due to the cavity. This translated to an increase of SNR by 30 dB for the beamforming measurements with respect to the flush mounted case.

In the near term, analysis needs to be performed on how the cavities, especially how the amplification seen with the hard walled cavity, array 2, affects the coherence of a sound source. Additionally, further work needs to be performed to understand why for the cavity design of array 4 at 20.2 $\mathrm{m\,s^{-1}}$ the TBL noise is attenuated more than that of the similar array 3 design.

This data establishes a framework for studying how different cavity geometries affect the accuracy and SNR of beamforming measurements. The end goal of this work is to identify a deterministic approach for optimizing cavities to improve aeroacoustic measurements in closed-section wind tunnels. This data will serve as the basis for future comparisons as well as be used to validate deterministic model predictions.

References

[1] Stoker, R., Guo, Y., Streett, C., and Burnside, N., "Airframe noise source locations of a 777 aircraft in flight and comparisons with past model–scale tests," *9th AIAA/CEAS Aeroacoustics Conference, May 12 – 14 2003, Hilton Head, South California, USA*, 2003, AIAA paper 2003–3232.

[2] Merino-Martinez, R., Sijtsma, P., Snellen, M., Ahlefeldt, T., Antoni, J., Bahr, C. J., Blacodon, D., Ernst, D., Finez, A., Funke, S., Geyer, T. F., Haxter, S., Herold, G., Huang, X., Humphreys, W. M., Leclère, Q., Malgoezar, A., Michel, U., Padois, T., Pereira, A., Picard, C., Sarradj, E., Siller, H., Simons, D. G., and Spehr, C., "A review of acoustic imaging methods using phased microphone arrays (part of the Aircraft Noise Generation and Assessment special issue)," *CEAS Aeronautical Journal*, Vol. 10, No. 1, March 2019, pp. 197–230, DOI: 10.1007/s13272-019-00383-4.

[3] Mueller, T., *Aeroacoustic Measurements*, Springer Science & Business Media, Berlin, Germany, 2002, ISBN: 978–3–642–07514–8.

[4] Merino-Martinez, R., van der Velden, W. C. P., Avallone, F., and Ragni, D., "Acoustic measurements of a DU96–W–180 airfoil with flow–misaligned serrations at a high Reynolds number in a closed–section wind tunnel," *7th International Meeting on Wind Turbine Noise, May 2 – 5 2017, Rotterdam, the Netherlands*, International Institute of Noise Control Engineering (I-INCE), 1A/B Westminster Chambers, 106 Lord Street, Southport PR8 1LF, United Kingdom, 2017.

[5] Merino-Martinez, R., Neri, E., Snellen, M., Kennedy, J., Simons, D. G., and Bennett, G. J., "Comparing flyover noise measurements to full–scale nose landing gear wind–tunnel experiments for regional aircraft," *23rd AIAA/CEAS Aeroacoustics Conference, June 5 – 9 2017, Denver, Colorado, USA*, 2017, AIAA paper 2017–3006.

[6] Fleury, V., Coste, L., Davy, R., Mignosi, A., Cariou, C., and Prosper, J.-M., "Optimization of Microphone Array Wall Mountings in Closed-Section Wind Tunnels," *AIAA Journal*, Vol. 50, No. 11, 2012, pp. 2325–2335.

[7] Jaeger, S. M., Horne, W., and Allen, C., "Effect of surface treatment on array microphone self–noise," *6th AIAA/CEAS Aeroacoustics Conference, June 12–14 2016, Lahaina, HI, USA*, 2000, AIAA paper 2000-1937.

[8] Vandercreek, C. P., Amiri-Simkooei, A., Snellen, M., and Ragni, D., "Experimental design and stochastic modeling of hydrodynamic wave propagation within cavities for wind tunnel acoustic measurements," *International Journal of Aeroacoustics*, Vol. 18, No. 8, 2019, pp. 752–779.

[9] Horne, W. C. and Burnside, N. J., "Development of new wall-mounted and strut-mounted phased microphone arrays for acoustic measurements in closed test-section wind tunnels," *21st AIAA/CEAS Aeroacoustics Conference*, 2015.

[10] Shin, H.-C., Graham, W. R., Sijtsma, P., Andreou, C., and Faszer, A. C., "Implementation of a Phased Microphone Array in a Closed-Section Wind Tunnel," *AIAA Journal*, Vol. 45, No. 12, December 2007, pp. 2897–2909.

[11] Horne, W. and James, K., "Concepts for reducing the self-noise of in-flow acoustic sensors and arrays," *5th AIAA/CEAS Aeroacoustics Conference and Exhibit*, No. c in Aeroacoustics Conferences, American Institute of Aeronautics and Astronautics, feb 1999.

[12] Rienstra, S. W., *Fundamentals of Duct Acoustics*, Technische Universiteit Eindhoven, 2015.

[13] Remillieux, M. C., Crede, E. D., Camargo, H. E., Burdisso, R. A., J., D. W., Rasnick, M., van Seeters, P., and Chou, A., "Calibration and Demonstration of the New Virginia Tech Anechoic Wind Tunnel," 14^{th} *AIAA/CEAS Aeroacoustics Conference (*29^{th} *AIAA Aeroacoustics Conference), May 5–7, 2008, Vancouver, British Columbia, Canada*, 2008, AIAA paper 2008–2911.

[14] van Veen, B. D. and Buckley, K. M., "Beamforming: A Versatile Approach to Spatial Filtering," *IEEE ASSP Magazine*, Vol. 5, No. 2, April 1988, pp. 4–24.

[15] Sijtsma, P., "Phased array beamforming applied to wind tunnel and fly–over tests," Tech. Rep. NLR–TP–2010–549, National Aerospace Laboratory (NLR), Anthony Fokkerweg 2, 1059 CM Amsterdam, P.O. Box 90502, 1006 BM Amsterdam, The Netherlands, December 2010.

[16] Sijtsma, P., Merino-Martinez, R., Malgoezar, A. M. N., and Snellen, M., "High–Resolution CLEAN–SC: Theory and Experimental Validation," *International Journal of Aeroacoustics*, Vol. 16, No. 4–5, 2017, pp. 274–298, SAGE Publications Ltd. London, United Kingdom.

[17] Merino-Martinez, R., Neri, E., Snellen, M., Kennedy, J., Simons, D. G., and Bennett, G. J., "Analysis of nose landing gear noise comparing numerical computations, prediction models and flyover and wind–tunnel measurements," 24^{th} *AIAA/CEAS Aeroacoustics Conference, June 25 – 29 2018, Atlanta, Georgia, USA*, 2018, AIAA paper 2018–3299.

[18] Merino-Martinez, R., Luesutthiviboon, S., Zamponi, R., Rubio Carpio, A., Ragni, D., Sijtsma, P., Snellen, M., and Schram, C., "Assessment of the accuracy of microphone array methods for aeroacoustic measurements," *Journal of Sound and Vibration*, Vol. 470, No. 115176, January 2020, pp. 1–24.

[19] Merino-Martinez, R., *Microphone arrays for imaging of aerospace noise sources*, Ph.D. thesis, Delft University of Technology, 2018, ISBN: 978–94–028–1301–2.

[20] Sarradj, E., "A Generic Approach to Synthesize Optimal Array Microphone Arrangements," *BeBeC*, 2016.

[21] Luesutthiviboon, S., Malgoezar, A., Snellen, M., Sijtsma, P., and Simons, D. G., "Improving Source Discrimination Performance by Using an Optimized Acoustic Array and Adaptive High–Resolution CLEAN–SC Beamforming," 7^{th} *Berlin Beamforming Conference, March 5 – 6 2018, Berlin, Germany*, GFaI, e.V., Berlin, 2018, BeBeC–2018–D07.

[22] G.R.A.S. Sound & Vibration – 40PH CCP Free–field array microphone, "http://www.gras.dk/products/special-microphone/array-microphones/product/178-40ph," Accessed in March 2017.

[23] G.R.A.S. Sound & Vibration – 42AA Pistonphone class 1, "https://www.gras.dk/products/calibration-equipment/reference-calibrator/product/255-42aa," Accessed in March 2017.

[24] Morse, P. M. and Ingard, K. U., *Theoretical acoustics*, McGraw-Hill, New York SE - xix, 927 pages illustrations 23 cm., 1968.

[25] Visaton – Speaker K 50 SQ – 8 Ohm, "http://www.visaton.de/en/products/fullrange-systems/k-50-sq-8-ohm," Accessed in March 2017.

[26] Merino-Martinez, R., Sijtsma, P., and Snellen, M., "Inverse Integration Method for Distributed Sound Sources," *7th Berlin Beamforming Conference, March 5 – 6 2018, Berlin, Germany*, GFaI, e.V., Berlin, 2018, BeBeC–2018–S07.

[27] Merino-Martinez, R., Sijtsma, P., Rubio Carpio, A., Zamponi, R., Luesutthiviboon, S., Malgoezar, A. M. N., Snellen, M., Schram, C., and Simons, D. G., "Integration methods for distributed sound sources," *International Journal of Aeroacoustics*, Vol. 18, No. 4–5, 2019, pp. 444–469.

[28] Merino-Martinez, R., Snellen, M., and Simons, D. G., "Functional beamforming applied to imaging of flyover noise on landing aircraft," *Journal of Aircraft*, Vol. 53, No. 6, November–December 2016, pp. 1830–1843.

[29] Lord Rayleigh, F. R. S., "XXXI. Investigations in Optics with special reference to the Spectroscope," *The London, Edinburgh and Dublin Philosophical Magazine and Journal of Science*, Vol. 8, No. 49, October 1879, pp. 261–274.

[30] Luesutthiviboon, S., Malgoezar, A. M. N., Merino-Martinez, R., Snellen, M., Sijtsma, P., and Simons, D. G., "Enhanced HR–CLEAN–SC for resolving multiple closely spaced sound sources," *International Journal of Aeroacoustics*, Vol. 18, No. 4–5, 2019, pp. 392–413.

[31] Horne, C., Hayes, J. A., Jaeger, S. M., and Jovic, S., "Effects of Distributed Source Coherence on the Response of Phased Acoustic Arrays," *6th AIAA/CEAS Aeroacoustics Conference, June 12 – 14 2000, Lyon, France*, 2000, AIAA paper 2000–1935.